

Effect of Friction Stir Welding on Microstructure and Mechanical Properties of UNS C19400 Alloy Plates

Floriano Martins^{a*} , Francisco M.F.A. Varasquim^b , Eli J. Cruz Junior^b,

Francisco Y. Nakamoto^a, Vinicius T. Santos^{c,d}, Jan Vatauvuk^d, Márcio R. Silva^c, Antonio A. Couto^{d,e},

Givanildo A. Santos^a 

^aInstituto Federal de Educação Ciência e Tecnologia de São Paulo (IFSP), Departamento de Engenharia Mecânica (SPO), São Paulo, SP, Brasil.

^bInstituto Federal de Educação Ciência e Tecnologia de São Paulo (IFSP), Departamento de Engenharia Mecânica (ITP), Itapetininga, SP, Brasil.

^cTermomecânica São Paulo S/A, Centro de Pesquisa e Desenvolvimento de Ensaios (CPDE), São Bernardo do Campo, SP, Brasil.

^dUniversidade Presbiteriana Mackenzie, Departamento Engenharia de Materiais, São Paulo, SP, Brasil.

^eInstituto de Pesquisas Energéticas e Nucleares (IPEN), São Paulo, SP, Brasil.

Received: May 11, 2023; Revised: September 27, 2023; Accepted: November 07, 2023

The welding of metallic materials by the Friction Stir Welding (FSW) method is a very attractive process for preserving their characteristics, especially for copper and its alloys that require high heat input and present many distortions by traditional methods. However, it is a great challenge to produce welds free of defects and maintain or improve their mechanical properties. In the current literature data on FSW parameters for copper and its alloys are scarce. In this study, tests were performed with a combination of four tool rotations (750, 850, 950, 1050 rev.min⁻¹) and two welding speeds (20 and 60 mm.min⁻¹), maintaining the tool inclination angle in 3° and waiting time of 5 seconds. The objective of this work is to analyze the microstructure and mechanical performance of lap joints of the UNS C19400 alloy joined by FSW. The process temperature was monitored to trace the heating profile of the process, in addition to microhardness and shear strength tests, in addition to optical microscopy for analysis. The joints welded by the parameters Ω 950 rev.mm⁻¹ v 20mm.min⁻¹ obtained a mechanical performance of 73% compared to the characteristics of the base metal and despite the appearance of volumetric defects at the microstructural level, the metallurgical transformations of recovery and recrystallization of the grains observed in the microstructure played a key role in the result.

Keywords: Copper-Iron Alloy, Mechanical Properties, Microstructure, Friction Stir Welding-FSW, Lap Joints.

1. Introduction

The intense search for materials obtained by ecologically correct methods is a call from society and a goal of industries today. The FSW technique differs from conventional methods because it requires low energy demand, does not produce fumes harmful to the operator's health and does not use filling material, being able to produce lighter products saving fuel and energy¹. Another advantage of the process is to produce joints of similar and dissimilar materials that would be difficult to weld using conventional methods, generating less distortion due to the low heat input offered compared to traditional methods². The aerospace, automobile, naval and energy industries are the main researchers and developers of the FSW technique³⁻⁷.

The FSW technique was developed by Thomas⁸ in 1991, by the British Institute of Welding (TWI) which over the

years has been gaining ground among researchers. This process uses only a non-consumable rotary tool of greater hardness than the material to be welded that penetrates the material until the shoulder touches the material. The friction between the parts generates heat, lower than the melting temperature, leaving the material in a paste state, so the tool runs longitudinally along the weld bead, plastically deforming the material and generating a stir flow^{3,9,10}, example shown in the Figure 1 the main process variables. According to Abdollah-Zadeh et al.¹² FSW is an *in-situ* extrusion and forging process.

In Figure 1, two working sides of the tool are shown, advancing side (AS) and retreating side (RS). The advanced side is when the tool velocity vector rotary agrees with the welding motion vector and the retraction side is when it happens the opposite of this^{1,9}. The advance side is where the disturbance in the material occurs, promoting deformation plastic of the material by raising the temperature and

*e-mail: floriartur@gmail.com

transforming the material into a semi-solid that is dragged to the indentation side¹³.

The FSW process has four regions of the weld bead shown in Figure 2, namely: Unaffected zone, heat affected zone (HAZ), thermo-mechanically affected zone (TMAZ), and stir zone (SZ)¹.

The FSW technique was initially developed for aluminum alloys and over the years, research has shown that it is possible to weld different materials, however, studies for copper and its alloys are still scarce in the literature^{14,15}, and according to Machniewicz et al.¹¹ parameters for copper and its alloys require further research as there is no consolidated literature, leaving a large gap for open studies. For the iron copper UNS C19400 alloy research for this process is scarce and it is one of the motivations of this work. For commercial applications of this alloy, it is essential to know the specific FSW process. Many advantages are associated with the

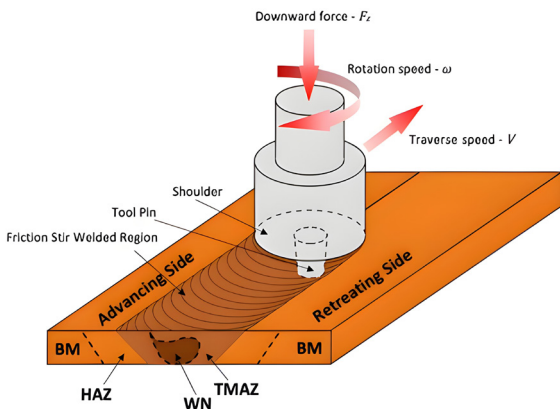


Figure 1. Schematic drawing of the FSW process¹¹.

FSW process, but there is no guarantee of producing defect-free welds and the challenges to produce quality joints are enormous, being fundamental the knowledge of the parameters involved^{19,16,17} and according to Albannai² the improper application of any parameters will generate visible or hidden defects.

Copper alloys have high thermal conductivity and to be soldered by conventional methods they demand a high thermal input, causing many defects and distortions and high residual stress and losing mechanical, thermal, and electrical properties¹⁸.

2. Materials and Methods

2.1. Materials

2.1.1. Sheet materials

UNS C19400 copper alloy sheets supplied in strips measuring 600 mm (length) x 100 mm (width) x 2 mm (thickness) were cut to dimensions 100 mm (length) x 20 mm (width) x 2 mm (thickness) to be mounted on a fixture base and assembled in the configuration for lap joints. The CuFe alloy, specifically UNS C19400 alloy, presents excellent hot and cold workability, high mechanical strength and electrical and thermal conductivity shown in Table 1.

The UNS C19400 alloy is resistant to natural, industrial, and marine atmospheres and because it contains Fe in its composition, its corrosion resistance is improved compared to pure copper. The other components of the alloy are shown in Table 2.

2.1.2. Tool material

One of the important points for the FSW process is the design of the tool, as its geometry influences the generation

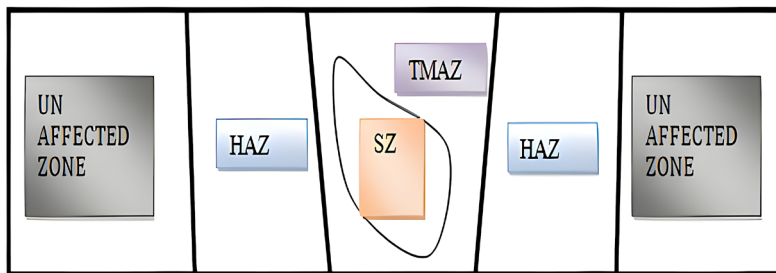


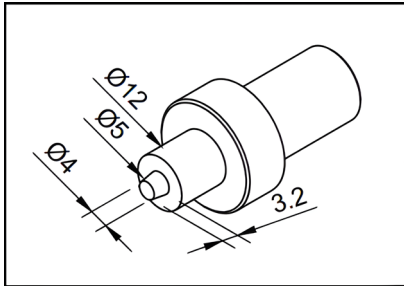
Figure 2. Characteristic zones of the FSW process. Unaffected zone, heat affected zone (HAZ), thermo-mechanically affected zone (TMAZ), and stir zone (SZ)¹.

Table 1. Properties and characteristics of the UNS C19400 alloy¹⁹.

Properties of the UNS C19400 alloy						
<i>T. Liquidus</i>	<i>T. Solidus</i>	Coefficient of linear thermal expansion (20°C to 300°C)	Thermal Conductivity (20°C)	Specific heat (20 °C)	Ultimate tensile strength	Yield strength
°C	°C	μ/m.K	W/m.K	J/kg.K	MPa	MPa
1090	1080	16.3	260	385	310-524	165-203

Table 2. Composition by weight of UNS C19400 alloy²⁰.

COMPOSITION (wt%)				
Cu	Fe	P	Zn	Pb
Bal.	2.1 – 2.6	0.015 – 0.15	0.05 – 0.2	0.03 max.

**Figure 3.** Tool details and dimensions.

of heat, the flow of the plasticized material^{15,9,11}, and also the force required for the longitudinal displacement of the tool²¹.

The tool basically consists of a fixation rod, shoulder and pin¹¹. The tool developed was made of heat-treated, quenched, and tempered H13 steel with a hardness of 50–56 HRC, with a simple truncated-cone geometry pin and its dimensions shown in Figure 3. Adopted the ratio between pin shoulder diameters = 3, widely used among researchers⁹.

2.2. Experiment arrangement

The joints were welded on a three-axis machining center from the company Veker, model MV 760 ECO with a total installed power of 15 kW. Fixing and assembly details are shown in Figure 4 and Figure 5.

2.2.1. Process temperature monitoring

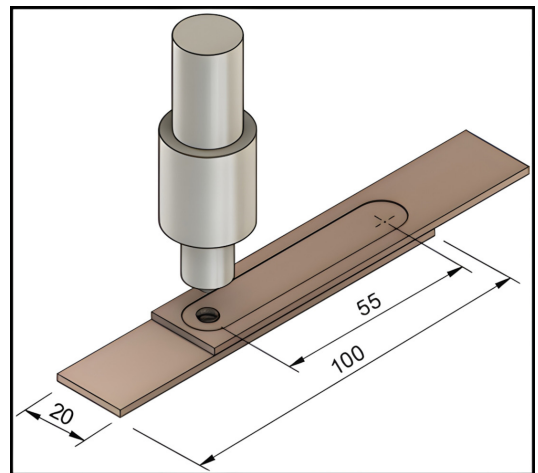
In order to monitor the process temperature, four K-type thermocouples were installed on the fixation base, placed 20 mm apart from each other, which maintained direct contact with the lower plate in the center of the weld line shown in Figure 6, and temperature monitoring was performed with a data logger developed with an Arduino® Uno board, connected to a computer via the USB port, and for reading the serial port, CoolTerm® software version 1.9.1 was used.

2.3. Process parameters

The range of initial parameters of this work were based on previous research on copper and its alloys, as there is still not enough work for the alloy under study. Compilation of FSW works is presented in Table 3.

For initial tests, four tool rotation speeds (Ω), 750, 850, 950, 1050 rev.mm⁻¹ and two welding speeds v , 20 and 60 mm.min⁻¹, tool inclination angle of 3° and dwell time after tool penetration of 5 seconds.

To carry out the tests, Minitab® software was used with application of the DOE tool – Planning of experiments, factorial 2^k, where k are the factors varying in two levels. The combination of parameters generated 8 tests and 4 replicates were adopted for each one, totaling 32 randomized experiments.

**Figure 4.** Fixing base assembly.**Figure 5.** Detail of the positioning of the plates.

2.4. Shear strength test

The shear strength test was performed like the works by Abdollah-Zadeh et al.¹² and Wiedenhoft et al.²², the schematic design is shown in Figure 7.

Table 3. Compilation of FSW works on copper sheets and their alloys.

Alloy/Class	thickness [mm]	Ω [rev.mm ⁻¹]	v [mm.min ⁻¹]	Reference
C 1XX	4	1250	61	Lee and Jung ²³
C 1XX	5	400 – 600 - 800	50	Xie et al. ²⁴
C 1XX	5	400 – 600 - 800	50	Xue et al. ²⁵
		800	50 – 100 - 200	
C 1XX	3	800-900	30 - 50	Hwang et al. ¹⁵
C 1XX	4	400 – 600 – 900 -1200 - 1250	25	Jabbari and Tutum ²⁶
C 1XX	5	600	75	Khodaverdizadeh et al. ²⁷
C 1XX	4	710	40	Teimurnezhad et al. ²⁸
C 1XX	8	800 – 1200 - 1600	5	Huaracán Pichún ²⁹
C1 XX – C 2XX	5	710 - 450	16 - 25	Gharavi et al. ³⁰
C 1XX	5	580	40 - 60 - 80	Machniewicz et al. ¹¹
C1 XX – C 3XX	6	1200	50	Saravanakumar et al. ³¹

Note: Ω = tool rotation, v = welding speed

In this test, force x displacement was monitored. A universal testing machine model DL-10000 with load capacity of 10000 kgf was used. The speed for this test was 2 mm.min⁻¹. To compare the results obtained from the welded specimens, a specimen of the same dimensions was used without welding and free of defects in the base metal.

2.5. Microhardness test

The points measured for the microhardness of the joint were collected in four different lines of the sample, as shown in Figure 8, where “Line 1” and “Line 2” are the lines of the lower plate and “Line 3” and “Line 4” are the lines of the upper plate, method adopted by Rosa et al.³² to measure microhardness in overlapping joints making it possible to investigate the direct influence on microhardness promoted by the heat generated by the shoulder and pin on the upper and lower plates. For this test, a Buehler microhardness tester was used on the Vickers HV 0.1 kgf scale and followed the ASTM E384³³ standard for Vickers hardness.

2.6. Metallographic preparation

Samples were taken from the region halfway along the longitudinal length of the weld bead, shown in Figure 9. The samples were embedded in Bakelite, sanded, and polished and the chemical etching to reveal the microstructure was HNO₃ + H₂O.

3. Results and Discussion

3.1. Checking the quality of the weld on the test specimens

The visual appearance analysis results of all tests are shown in Table 4.

The specimens welded with the parameters $\Omega = 950$ rev.mm⁻¹, and $v = 20$ mm.min⁻¹ had the best visual appearance, that is, by the adopted quality criterion of not presenting defects visible to the naked eye and for these were made characterization tests such as micrography, microhardness, shear resistance. The visual appearance is shown in Figure 10.

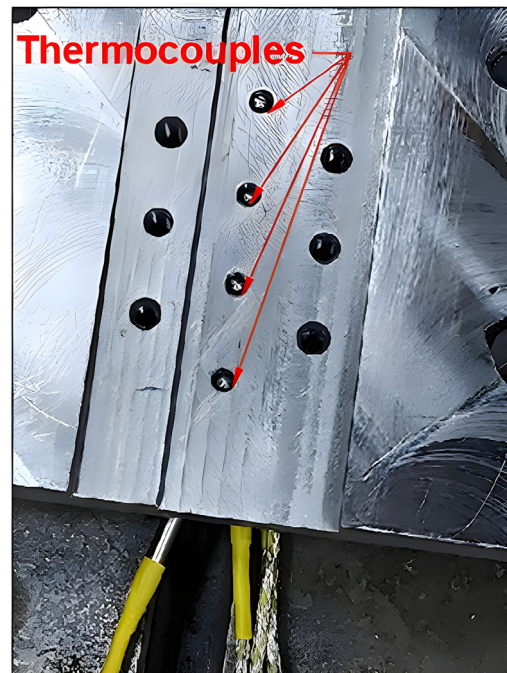


Figure 6. Positioning of thermocouples on the fixing base.

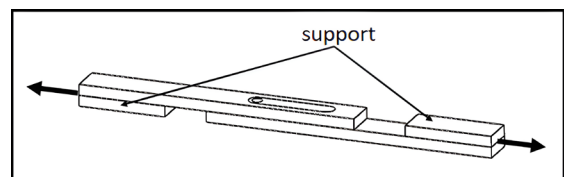


Figure 7. Schematic drawing of the shear strength test²².

3.2. Process temperature profile

Monitoring the temperature distribution of the process is paramount but capturing it directly in the stir zone is very difficult due to the intense plastic deformation of the material,

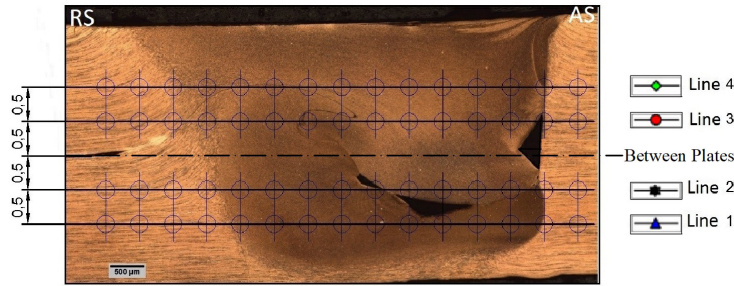


Figure 8. Line of points (pitch: 0.5 mm) and vertical distances 0.5 mm for microhardness testing. Note: RS = Retraction Side, AS= Advancing Side.

Table 4. Test results, visual quality analysis.

Ω [rev.mm ⁻¹]	v [mm.min ⁻¹]	Results
750	20	Tool collapse; great tunnels
	60	Tool collapse
850	20	Small pores on the surface
	60	Pores and small tunnels on the surface
950	20	No visible defects
	60	Small pores on the surface
1050	20	Small pores on the surface and flash
	60	Tool collapse; small tunnels

Table 5. Maximum FSW process temperatures for UNS C19400 alloy.

Thermocouple	Standard Deviation	Maximum Temperature °C
T1 (tool input and dwell time 5 s)	30.34	429.65
T2 (intermediary1)	16.06	378.6
T3 (intermediary2)	24.77	369.8
T4 (tool output)	14.94	338.2

the temperature being estimated by the microstructure generated or by thermocouples installed very close to it¹⁴. Figure 4 shows the temperature profile of the process where thermocouple T1 refers to the first thermocouple, beginning of the process and thermocouples T2 and T3 are intermediate and thermocouple T4 is located at the end of the process. The first thermocouple is the one that reaches the highest temperature of approximately 447 °C due to the initial friction and the waiting time of 5 seconds for the start of the longitudinal displacement of the tool. As shown in Figure 4, it corroborates with the authors Kumar et al.³ and Anand and Sridhar¹ that the FSW process reaches temperatures much lower than the melting temperature of the material, which for this alloy is 1090 °C.

The average maximum temperatures observed by each thermocouple are shown in Table 5. The first thermocouple reaches the highest temperature due to the tool entry and shoulder contact with the plate for 5 seconds. Monitoring the temperature throughout the process allowed the printing

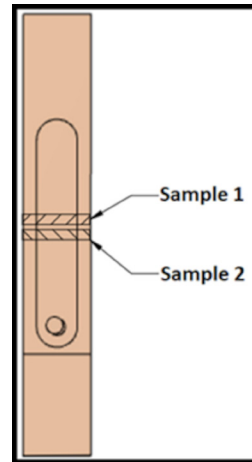


Figure 9. Position of sample withdrawal for micrography.



Figure 10. Test specimens welded with Ω 950 rev.mm⁻¹ and v 20 mm.min⁻¹.

of the process heating profile graph for the alloy, shown in Figure 11.

3.2. Shear resistance test- results

Four specimens with the parameters Ω 950 rev.mm⁻¹ v 20mm.min⁻¹ were submitted to the test, additionally two welded specimens were tested with the parameters Ω 850 rev.mm⁻¹ v 60mm.min⁻¹ and Ω 850 rev.mm⁻¹ v 20mm.min⁻¹, shown in Figure 12. The motivation for inclusion was the appearance

of defects visible to the naked eye in these samples and the curiosity about the influence on the performance of the joint.

The result of the shear strength test is shown in Table 6. The results were compared with Base metal intact and weldless specimen. The specimens with the parameters $\Omega = 950 \text{ rev.mm}^{-1}$ and $\mathbf{v} = 20 \text{ mm.min}^{-1}$ obeyed a standard with an average performance of 73%, specimen-5 65%

Table 6. Maximum force reached by the specimens in the shear resistance test.

Specimen	Maximum force [N]	Elongation [%]
Base metal	14874.16	6.20
Specimen-1	11675.48	5.02
Specimen -2	10136.56	4.82
Specimen -3	10289.18	5.18
Specimen -4	11799.49	5.48
Specimen -5	9685.05	4.68
Specimen -6	11872.62	5.92

Note: Specimen 1 to specimen 4 were welded with the parameters $\Omega = 950 \text{ rev.mm}^{-1}$ and $\mathbf{v} = 20 \text{ mm.min}^{-1}$, specimens 5 and 6 were welded with the parameters $\Omega = 850 \text{ rev.mm}^{-1}$ and $\mathbf{v} = 60 \text{ mm.min}^{-1}$; and $\Omega = 850 \text{ rev.mm}^{-1}$ and $\mathbf{v} = 20 \text{ mm.min}^{-1}$, respectively.

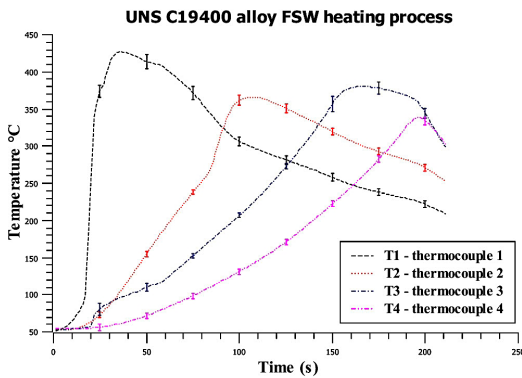


Figure 11. FSW process heating profile for UNS C19400 alloy.

and specimen-6 with 80%, observing the maximum force, showing that defects that are visually present in a sample do not a priori indicate lack of performance.

3.3. Microhardness

The result of the microhardness test is shown in the graph of Figure 13. For comparison with a standard, measurements were made on the base material, obtaining an average of 130.5 HV. A smoothing of the microhardness is clearly noticed in the center of the joint where the SZ and in TMAZ and HAZ a slight difference is noticed between the AS and the RS.

We believe that microhardness softening was caused mainly by the intense plastic deformation and the supply of heat directly to the microstructure, causing a metallurgical transformation, becoming more evident in the Microstructure chapter.

3.4. Microstructure

The optical micrographs are shown in Figure 14, where the main image identified the zones affected by heat, as well as the advancing and retracting sides. The other images were captured with greater magnification to verify greater details. Analyzing then it can be noticed some defects like a Hook-type in the SZ region (Figure 14b), tunnels (Figure 14f and Figure 14g) in addition some ampliations show a microstructural details like a lower central transition of the joint, with part of the homogeneous SZ (Figure 14c) and equiaxed grains in the central zone of the SZ (Figure 12d and e), it happens because of the heat supplied directly to the microstructure of the joint.

3.5. Defects

For this work, samples welded with $\Omega 950 \text{ rev.mm}^{-1}$ and $\mathbf{v} 20 \text{ mm.min}^{-1}$ were adopted because they presented a uniform welding and free of defects to the naked eye, but it was evidenced in the test of micrograph images innumerable defects inherent to the process, it is believed that due to the flow of inadequate material generated by the tool. Images d), f) and g) of Figure 14 show kissing bond, tunnel, voids, and fragmented material defects, respectively.



Figure 12. Welded samples with parameters $\Omega 850 \text{ rev.mm}^{-1}$ $\mathbf{v} 60 \text{ mm.min}^{-1}$ and $\Omega 850 \text{ rev.mm}^{-1}$ $\mathbf{v} 20 \text{ mm.min}^{-1}$ respectively, defects in details.

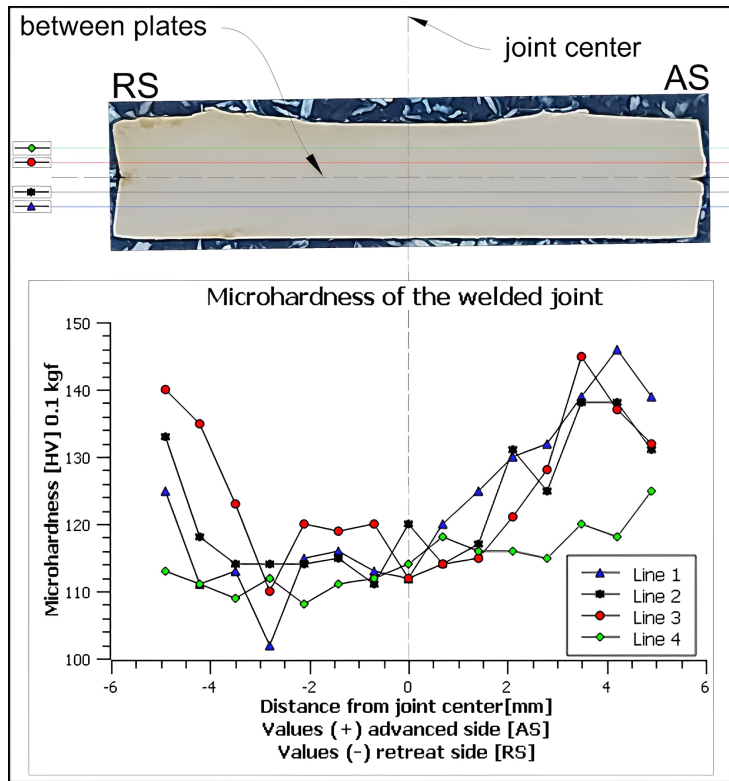


Figure 13. Microhardness profile of the FSW welded joint $\Omega = 950 \text{ rev.mm}^{-1}$ and $v = 20 \text{ mm.min}^{-1}$.

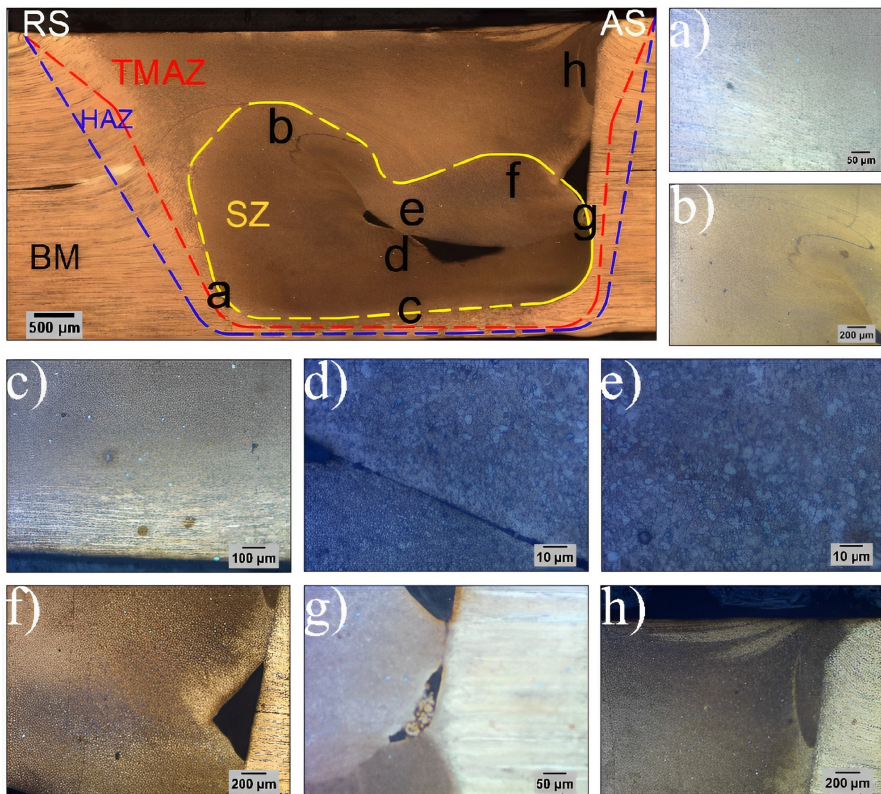


Figure 14. Joint microstructure $\Omega = 950 \text{ rev.mm}^{-1}$ and $v = 20 \text{ mm.min}^{-1}$.

4. Conclusions

The analysis of the tests allowed reaching some conclusions, despite the presence of several types of defects in the microstructure, the joints had a good mechanical performance against the material without welding. The specimen with defects at the macro level with the parameters $\Omega = 850 \text{ rev.mm}^{-1}$ and $\mathbf{v} = 20 \text{ mm.min}^{-1}$ performed well, while the specimen welded with the parameters $\Omega = 850 \text{ rev.mm}^{-1}$ and $\mathbf{v} = 60 \text{ mm.min}^{-1}$ obtained an unsatisfactory performance, it is believed that due to the higher welding speed it was not possible for the tool to generate an adequate flow of the plasticized material directly influencing the microstructure.

All specimens ruptured in the tool exit hole, which despite being inherent to the process is considered a defect and proved to be a point of greater stress concentration than the others.

The material from the stir zone showed a smoothing of the microhardness, in relation to the material in the initial state, mainly in the stir zone and subtly on the retraction side.

The microstructure features equiaxed grains in the stir zone due to the heat supplied directly to the microstructure.

This research was successful in joining the UNS-C19400 copper sheets, being a start for new research to improve the quality of the welding, such as new tool profiles and parameters.

The FSW process proved to be efficient in the processing of materials, as with low energy demand it was possible to transform the microstructure obtaining a gain in mechanical and metallurgical properties.

5. Acknowledgements

We thank IFSP and Termomecanica São Paulo S.A. for the opportunity to carry out this work.

This study was financed in part by the Coordenação de Aperfeiçoamento de Pessoal de Nível Superior – Brasil (CAPES).

6. References

- Anand R, Sridhar V. Studies on process parameters and tool geometry selecting aspects of friction stir welding—A review. *Mater Today Proc.* 2020;27:576-83. <http://dx.doi.org/10.1016/j.matpr.2019.12.042>.
- Albannai A. Review the common defects in friction stir welding. *Int J Sci Technol Res.* 2020;9:318-29.
- Kumar S, Mahajan A, Kumar S, Singh H. Friction stir welding: Types, merits & demerits, applications, process variables & effect of tool pin profile. *Mater Today Proc.* 2022;56:3051-7. <http://dx.doi.org/10.1016/j.matpr.2021.12.097>.
- Shash AY, El-Moayed MH, Abd Rabou M, El-Sherbiny MG. A coupled experimental and numerical analysis of AA6063 friction stir welding. *Proc Inst Mech Eng, C J Mech Eng Sci.* 2022;236(15):8392-400. <http://dx.doi.org/10.1177/09544062221085884>.
- El-Sayed MM, Shash A, Abd-Rabou M, El-Sherbiny MG. Welding and processing of metallic materials by using friction stir technique: a review. *J Adv Join Process.* 2021;3:100059. <http://dx.doi.org/10.1016/j.jajp.2021.100059>.
- El-Sayed M, Shash A, Abd Rabou M. Heat transfer simulation and effect of tool pin profile and rotational speed on mechanical properties of friction stir welded AA5083-O. *J Weld Join.* 2017;35(3):35-43. <http://dx.doi.org/10.5781/JWJ.2017.35.3.6>.
- El-Sayed MM, Shash AY, Mahmoud TS, Rabbou MA. Effect of friction stir welding parameters on the peak temperature and the mechanical properties of aluminum alloy 5083-O. In: Öchsner A, Altenbach H, editors. *Improved performance of materials: design and experimental approaches.* Cham: Springer; 2018. p. 11-25. http://dx.doi.org/10.1007/978-3-319-59590-0_2.
- Thomas WM. Friction stir butt welding. United Kingdom. UK PCTGB9202203. 1991.
- Khan N, Rathee S, Srivastava M. Friction stir welding: an overview on effect of tool variables. *Mater Today Proc.* 2021;47:7196-202. <http://dx.doi.org/10.1016/j.matpr.2021.07.487>.
- Verma M, Ahmed S, Saha P. Challenges, process requisites/inputs, mechanics and weld performance of dissimilar microfriction stir welding (dissimilar μ FSW): a comprehensive review. *J Manuf Process.* 2021;68:249-76. <http://dx.doi.org/10.1016/j.jmapro.2021.05.045>.
- Machniewicz T, Nosal P, Korbel A, Hebda M. Effect of FSW traverse speed on mechanical properties of copper plate joints. *Materials.* 2020;13(8):1937. <http://dx.doi.org/10.3390/ma13081937>.
- Abdollah-Zadeh A, Saeid T, Saizgari B. Microstructural and mechanical properties of friction stir welded aluminum/copper lap joints. *J Alloys Compd.* 2008;460(1-2):535-8. <http://dx.doi.org/10.1016/j.jallcom.2007.06.009>.
- Medeiros WW. Análise da influência da soldagem por fricção e atrito de ligas de alumínio [thesis]. São Paulo: Instituto Federal de Educação, Ciência e Tecnologia de São Paulo; 2020.
- Mishra RS, Ma Z. Friction stir welding and processing. *Mater Sci Eng Rep.* 2005;50(1-2):1-78. <http://dx.doi.org/10.1016/j.mser.2005.07.001>.
- Hwang Y, Fan P, Lin C. Experimental study on friction stir welding of copper metals. *J Mater Process Technol.* 2010;210(12):1667-72. <http://dx.doi.org/10.1016/j.jmatprotec.2010.05.019>.
- Al-Moussawi M, Smith A. Defects in friction stir welding of steel. *Metallogr Microstruct Anal.* 2018;7(2):194-202. <http://dx.doi.org/10.1007/s13632-018-0438-1>.
- El-Moayed MH, Shash AY, Rabou MA, El-Sherbiny MG. A detailed process design for conventional friction stir welding of aluminum alloys and an overview of related knowledge. *Eng Rep.* 2021;3(2):e12270. <http://dx.doi.org/10.1002/eng.2.12270>.
- Bisadi H, Tavakoli A, Sangsaraki MT, Sangsaraki KT. The influences of rotational and welding speeds on microstructures and mechanical properties of friction stir welded Al5083 and commercially pure copper sheets lap joints. *Mater Des.* 2013;43:80-8. <http://dx.doi.org/10.1016/j.matdes.2012.06.029>.
- ASM Handbook Committee. Properties and selection: nonferrous alloys and special purpose materials. Vol. 2. Materials Park: ASM International; 1990.
- ASTM: American Society for Testing and Materials. ASTM B465-20: standard specification for copper-iron alloy plate, sheet, strip, and rolled bar. West Conshohocken: ASTM Internacional; 2020.
- Chatha JS, Shahi A, Handa A. Stir welding parameters effect on flat plates weld joints: a review. *Mater Today Proc.* 2021;43:158-63. <http://dx.doi.org/10.1016/j.matpr.2020.11.396>.
- Wiedenhof AG, Amorim HJ, Rosendo TS, Tier MAD, Reguly A. Effect of heat input on the mechanical behaviour of Al-Cu FSW lap joints. *Mater Res.* 2018;21(4):e20170983. <http://dx.doi.org/10.1590/1980-5373-mr-2017-0983>.
- Lee WB, Jung SB. The joint properties of copper by friction stir welding. *Mater Lett.* 2004;58(6):1041-6. <http://dx.doi.org/10.1016/j.matlet.2003.08.014>.
- Xie G, Ma Z, Geng L. Development of a fine-grained microstructure and the properties of a nugget zone in friction stir welded pure copper. *Scr Mater.* 2007;57(2):73-6. <http://dx.doi.org/10.1016/j.scriptamat.2007.03.048>.
- Xue P, Xie G, Xiao B, Ma Z, Geng L. Effect of heat input conditions on microstructure and mechanical properties of friction-stir-welded pure copper. *Metall Mater Trans, A Phys Metall Mater Sci.* 2010;41(8):2010-21. <http://dx.doi.org/10.1007/s11661-010-0254-y>.

26. Jabbari M, Tutum CC. Optimum rotation speed for the friction stir welding of pure copper. *Int Sch Res Notices*. 2013;2013:978031. <http://dx.doi.org/10.1155/2013/978031>.
27. Khodaverdizadeh H, Heidarzadeh A, Saeid T. Effect of tool pin profile on microstructure and mechanical properties of friction stir welded pure copper joints. *Mater Des*. 2013;45:265-70. <http://dx.doi.org/10.1016/j.matdes.2012.09.010>.
28. Teimurmezhad J, Pashazadeh H, Masumi A. Effect of shoulder plunge depth on the weld morphology, macrograph and microstructure of copper FSW joints. *J Manuf Process*. 2016;22:254-9. <http://dx.doi.org/10.1016/j.jmapro.2016.04.001>.
29. Huaracán Pichún CA. Factibilidad técnica de realizar soldadura por fricción-agitación (FSW) en cobre puro, para centro de mecanizado CNC, CCHEN. Santiago de Chile: Universidad de Chile; 2018.
30. Gharavi F, Ebrahimzadeh I, Amini K, Sadeghi B, Dariya P. Effect of welding heat input on the microstructure and mechanical properties of dissimilar friction stir-welded copper/brass lap joint. *Mater Res*. 2019;22(4):e20180599.
31. Saravanakumar S, Vinoth kumar H, Franklin BA, Saravanan M, Siddharth J. Experimental analysis of dissimilar metal of copper and brass plates fabricated friction stir welding. *Mater Today Proc*. 2020;33:3131-4.
32. Rosa RF, Almeida IO, Varasquim FM, Cruz EJ Jr, Couto AA, Santos VT, et al. Analysis of the influence of friction stir welding on the microstructure and mechanical properties of alloy UNS-C27200 (CU-ZN). *Mater Res*. 2023;26(Suppl 1):e20220581. <http://dx.doi.org/10.1590/1980-5373-mr-2022-0581>.
33. ASTM: American Society for Testing and Materials. ASTM E384-17: standard test method for microindentation hardness of materials. West Conshohocken: ASTM Internacional; 2017.